

Research Article

Improving Our Knowledge of the Solar Near-Surface Shear Layer: The Special Case of the Leptocline

Jean Pierre Rozelot¹, Alexander Kosovichev^{2,3}, Irina Kitiashvili³

1. Université de la Côte d'Azur, France; 2. Center for Computational Heliophysics, New Jersey Institute of Technology, United States; 3. NASA Ames Research Center, USA

The discovery of the solar activity cycle was linked from the outset to the observation of the temporal variability of sunspots, which we know to be the result of complex processes associated with the dynamics of inner layers. Numerous recent studies have highlighted changes in the Sun's Near-Surface Shear Layer (NSSL), pointing to the role of the leptocline, a shallow and sharp rotational shear layer in the top ~ 8 Mm. The leptocline, mainly characterized by a strong radial rotational gradient at middle latitudes and self-organized meridional flows, is the cradle of numerous phenomena: opacity, superadiabaticity, and turbulent pressure changes; the hydrogen and helium ionization processes; a sharp decrease in the sound speed; and, probably, variations of the seismic radius associated with a nonmonotonic expansion of subsurface layers with depth. In addition, the leptocline may play a key role in forming the magnetic butterfly diagram. Such results are a starting point for further systematic investigations of the structure and dynamics of this layer, which will lead to a better understanding of solar activity.

1. Introduction

In recent years, numerous studies have focused on the physical conditions prevailing in the Sun's subsurface layers for at least two reasons. The first addresses the problem of how both the physical conditions in subsurface layers of the Sun and the nature of the magnetic flux tubes of active regions are reflected in the structure and behavior of these regions at the surface (e.g. Howard^[1]; Choudhuri and Jha^[2]; Rabello Soares et al.^[3]; Kitchatinov^[4]; Vasil et al.^[5]). The second relates to differential rotation: the aim is to understand how the solar rotation, which is not uniform in latitude, also varies

in depth and time. One of the most intriguing features is the rotation rate, which is faster at the equator than at the pole, a phenomenon known as “differential rotation” (for instance and references therein Javaraiah and Gokhale^[6]; Javaraiah^[7]; Tassoul^[8]; Howe^[9]).

Let us recall that the radiative interior of the Sun and its convective zone are separated, at a depth of around $0.7R_{\odot}$, by a thin layer ($\approx 0.05R_{\odot}$) at which the stratification changes rapidly from convective stability to marginal instability. This region shows a relatively sharp change between the solid-body rotation of the radiative interior and the differential rotation of the convection zone that Spiegel and Zahn^[10] termed the tachocline.

Helioseismic studies, which are a powerful tool for probing the solar interior in three dimensions, show significant velocity variations in the near-surface layers. The treatment of the superadiabatic region supposes a proper description of turbulent convection and detailed radiative energy transport and thermodynamic calculations. We also need to understand how the turbulent convection interacts with solar rotation. Furthermore, helioseismic studies have illustrated that the most significant changes with the solar cycle occur in a near-surface shear layer (NSSL), occupying around 5% of the solar radius at the top of the convection zone. The velocity shear may convert a part of the poloidal magnetic field into the toroidal field, and, in addition to the global dynamo operating in the bulk of the convection zone (e.g. Pipin et al.^[11]), the magneto-rotational instability may play a certain role^[5].

Helioseismic observations and numerical simulations reveal the existence of a shallow sub-surface ~ 8 Mm deep layer at the top of the NSSL^{[12][3]}. By analogy to the tachocline, this layer is called “leptocline”^[13], from the Greek “leptos”, thin and “klino”, tilt, or slope. This paper aims to present a new analysis of the gradient of solar rotation using global helioseismology data from the Solar and Heliospheric Observatory (SoHO) and Solar Dynamics Observatory (SDO) and highlight the role of the leptocline in our understanding of the structure and dynamics of the Sun and their variations with the solar activity cycles.

2. Radial Gradients of Solar Rotation: Tachocline and Leptocline

The internal rotation of the Sun has been observed almost uninterruptedly since 1996 from two space missions, the Solar and Heliospheric Observatory (SoHO)^[14] and the Solar Dynamics Observatory (SDO)^[15] as well as from the ground-based Global Oscillation Network Group (GONG) network^[16]. The

rotation rate is inferred by applying helioseismic inversion techniques to the rotational splitting of solar oscillation frequencies measured every 72 days from Doppler velocity images^[17].

Figure 1a shows the solar rotation rate, Ω , averaged over all available 141 inferences in 1996–2024 from SoHO and SDO, which are available from Joint Science Operation Center at Stanford¹¹<http://jsoc.stanford.edu>^[18]. The gray areas in this image shows the regions of uncertainty where the averaging kernels of the helioseismic inversions are not well-localized^[19]. The logarithmic radial gradient of the rotation rate averaged over the same period is shown in Figure 1b. The bottom panels (Fig. 1c-d) show the radial dependencies of Ω and $d\log \Omega/d\log r$ for several latitudes. The error bars show the standard deviations of the weighted averages.

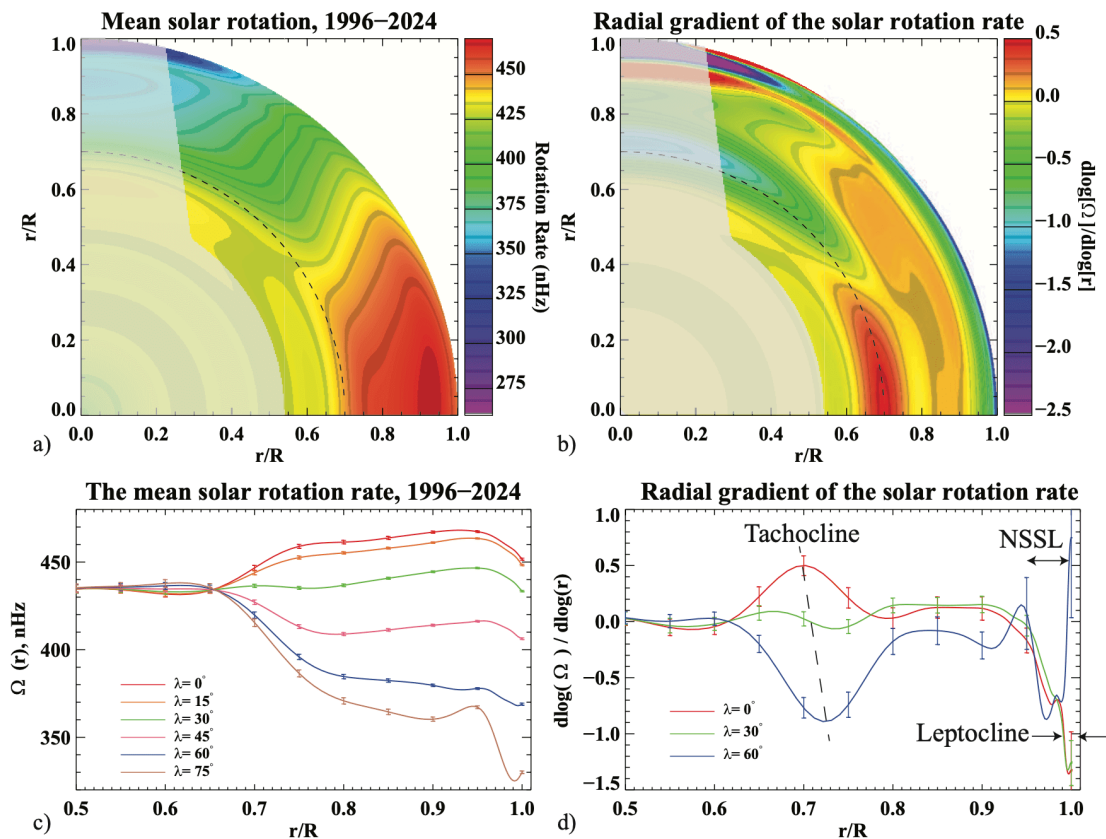


Figure 1. The mean rotation rate, Ω , and the radial gradient, $d\log \Omega/d\log r$, averaged over all SoHO/MDI and SDO/HMI measurements in 1996–2024, as a function of radius and latitude. a-b) cross-section views of the rotation rate and the gradient (the shaded region is where the inversion results are uncertain); c) the mean rotation rate at six latitudes indicated in the figure; d) the radial gradient as a function of radius at three latitudes indicated in the figure.

These results are generally consistent with previous inferences of the internal solar rotation^{[20][21][19]}. In particular, the results reveal two zones of sharp gradients at the bottom of the convection zone (the tachocline) and its top (the Near-Surface Shear Layer, NSSL). The gradient maximum values at the equator and 60 degrees latitude, connected by a dashed line in Fig. 1d, indicated that the tachocline is deeper at the equator than at the high latitude by about $0.02-0.03 R_{\odot}$. This means the tachocline has a prolate shape as initially argued by Gough and Kosovichev^[22].

The basic features of the internal solar rotation can be summarized as follows:

- Below $0.68 R_{\odot}$, the radiative interior rotates almost rigidly at a rate of about 430 nHz.
- The transition from the uniformly rotating radiation zone to a differentially rotating convection zone occurs in a thin layer from 0.68 to $0.73 R_{\odot}$. This layer is called the tachocline.
- In the bulk of the convection zone ($0.73 R_{\odot} < r < 0.96 R_{\odot}$), the rotation rate varies strongly with latitude. The equator rotates about 30% faster than the poles, from ~ 460 nHz at 0° latitude to ~ 340 nHz at 80° latitude.
- The contours of constant angular velocity are inclined by about 25° with respect to the rotational axis over a wide range of latitudes, i.e., rotation does not follow the Taylor-Proudman theorem.
- In a shallow layer, between $0.96 R_{\odot}$ and $1 R_{\odot}$, the rotation rate decreases by about 5% at all latitudes, showing however a more complex behavior near the surface. This layer is called the Near Subsurface Shear Layer (NSSL).
- A substructure of the NSSL, the leptocline, located just below the surface, covers about 8 Mm in depth within the convection zone ($0.985 R_{\odot} < r < 1.0 R_{\odot}$).
- The leptocline unfolds an intricate behavior of the variation of the radial gradient, $d\log \Omega / d\log r$, in latitude, depth, and in time.

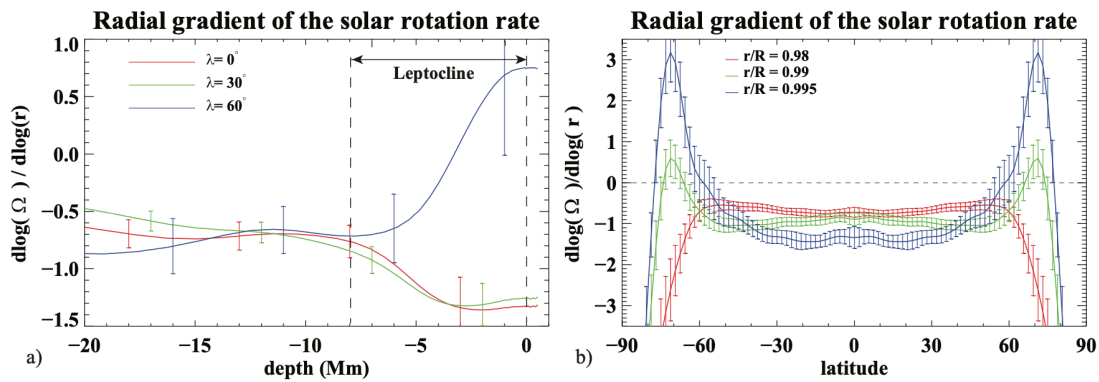


Figure 2. The radial gradient of the mean rotation rate, averaged over all SoHO/MDI and SDO/HMI measurements in 1996–2024, as a function of depth in the near-surface shear layer at 0° , 30° , and 60° latitudes.

Figure 2 shows the radial gradient in the leptocline as a function of depth and latitude in more detail. The gradient that remains constant, ≈ -1 , in the deep NSSL sharply increases its negative value to ≈ -1.5 in the leptocline at the equator and low latitudes. But, at higher latitudes the gradient becomes positive, so that the rotation rate increases towards the surface. The gradient is constant in a top 2–3 Mm deep layer in these inversion results. However, we must emphasize that these are the global helioseismology inversions that include only the oscillation modes with an angular degree of up to 300. These data do not resolve sharp variations near the surface, smoothed with so-called averaging kernels (e.g. Schou et al.^[19]). Therefore, the actual gradients of the rotation rate may be significantly larger than those revealed by the helioseismic inversions.

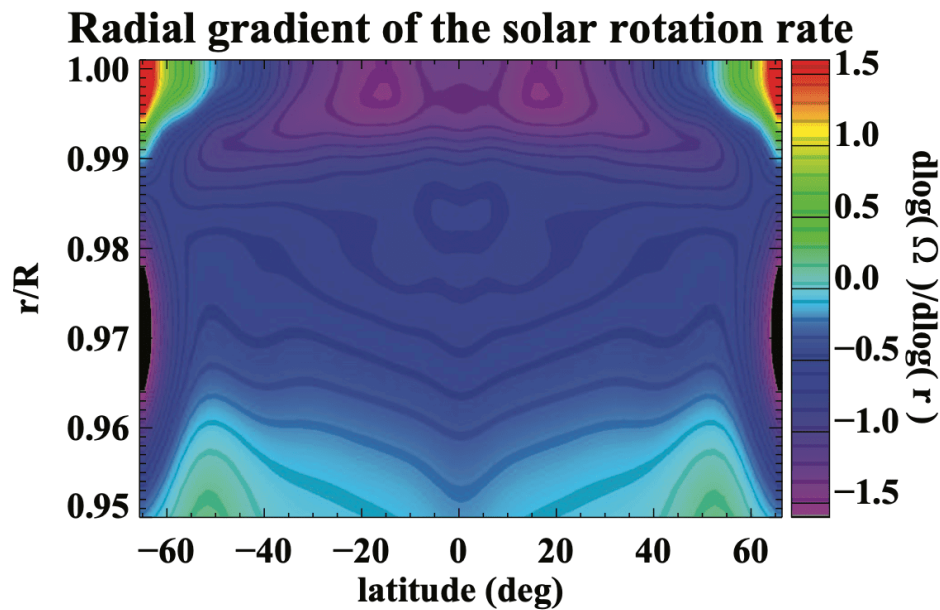


Figure 3. Variations of the rotational gradient, $d\log \Omega / d\log r$, in the leptocline a) with the depth below the solar surface at three latitudes, and b) with latitude at three depths (shown in the figure); c) latitude-radius diagram of the rotational gradient in the NSSL and leptocline.

In fact, recent local helioseismology measurements based on the ring-diagram analysis that involved oscillation modes of high angular degree showed that the gradient at low latitudes can reach values of $\simeq -2.6$ at a depth of about 3 Mm and then reverse to smaller values at the surface^{[23][3]}. The latitude-radius diagram of the mean rotational gradient shown in Figure 3 is qualitatively similar to the diagram obtained from the ring-diagram analysis (Figure 5 in Komm^[23]). Nevertheless, there are significant differences, particularly in the latitudinal structure of the NSSL and the leptocline. For instance, the reversal of the gradient values from negative to positive at about 60° latitudes in the leptocline is prominent in the global helioseismology data. The ring-diagram analysis showed such reversal but in deeper layers below the leptocline. Such discrepancy must be resolved in future studies.

3. Solar-Cycle Variations of the Rotational Gradient

Differential rotation also varies with time and typically reflects the solar cycle. After subtracting the mean rotation, the residual component revealed alternating zones of fast and slow flow bands, discovered by Howard and Labonte^[24] and called “torsional oscillations” because of their cyclic

variations. The zonal flows originate at mid-latitudes and form two branches migrating toward the equator and polar regions just like the magnetic butterfly diagram but with the overlapping “extended” 22-year cycles^[25].

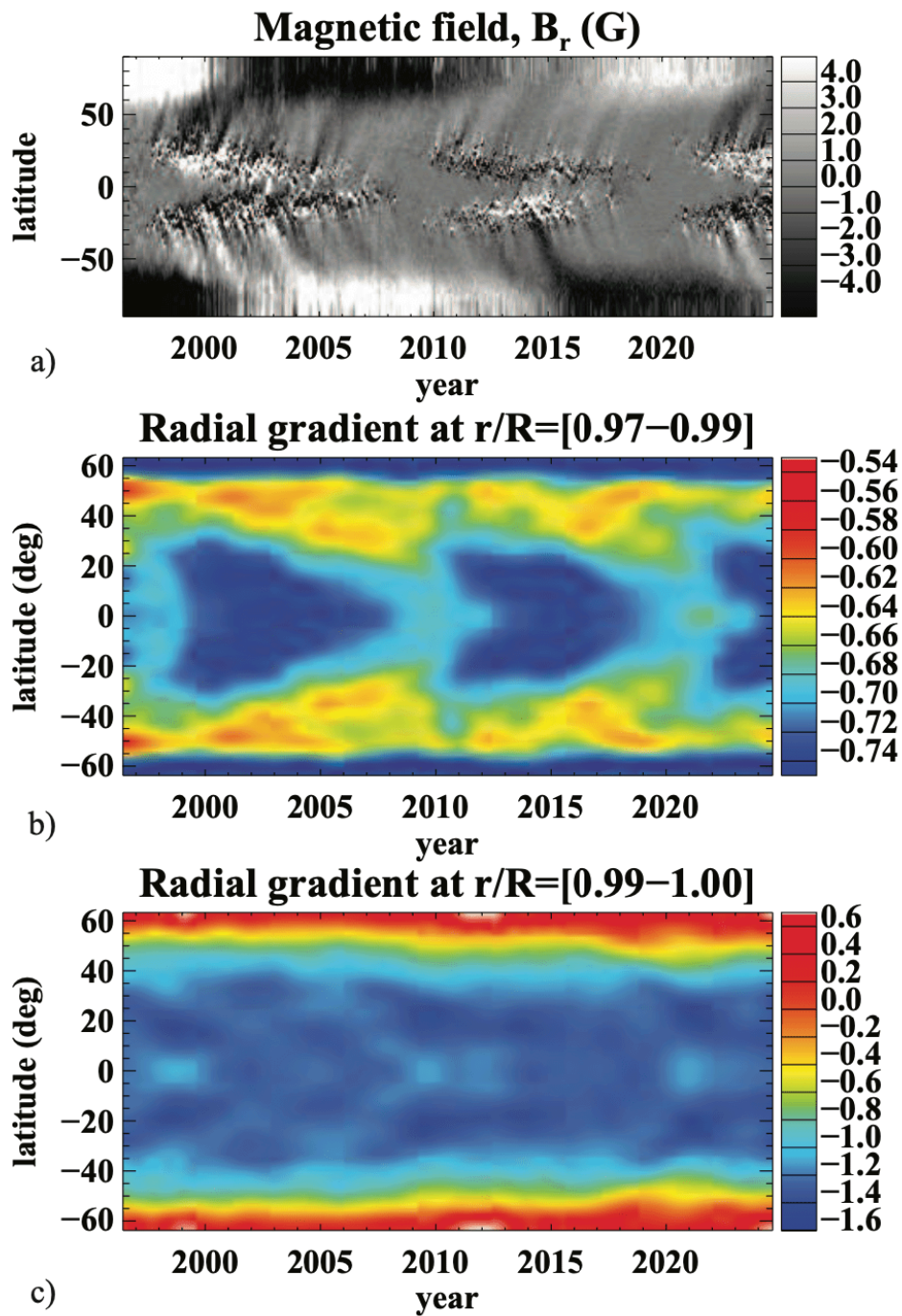


Figure 4. a) The magnetic time-latitude (“butterfly”) diagram for the radial component of the line-of-sight magnetic field from the SoHO and SDO data; b-c) the time-latitude diagrams for the rotational gradient, $d\log \Omega/d\log r$ below the leptocline ($r/R = 0.97 - 0.99$) and in the leptocline ($r/R = 0.99 - 1.00$) respectively.

Previous analyses of the internal rotation showed that the extended solar cycle represents the dynamo waves originating at the bottom of the convection zone and migrating towards the surface^{[26][27]}. The dynamo model of Pipin and Kosovichev^[28] showed that these zone flows are due to the action of dynamo-generated magnetic fields and their effects on the convective heat transport and the meridional circulation in the solar convection zone. Both the observational data and the dynamo model show that the near-shear shear layer plays a key role in the formation of the magnetic butterfly diagram. The role of the leptocline in the solar dynamo has not yet been established. However, this shallow subsurface region is critical for the process of formation of sunspots and active regions.

To illustrate the solar-cycle variations in the NSSL and leptocline, in Figure 4 we present the variations of the radial gradient as a function of time and latitude in two layers, just below the leptocline, at $r/R_{\odot} = 0.97 - 0.99$ (or in the depth range of 7-21 Mm) and in the leptocline (panel b), at $r/R_{\odot} = 0.99 - 1.00$ (the corresponding depth range is 0-7 Mm (panel c)). The comparison with the corresponding magnetic butterfly diagram (panel a) shows that below the leptocline, the negative gradient becomes stronger (dark blue areas in panel b) in the strong magnetic field regions migrating toward the equator and weaker in the high-latitude regions during the sunspot cycles. In the leptocline (panel c), the variations are less pronounced and have more complicated structures, which, however, resemble the overlapping extended cycles of the torsional oscillations. In particular, the rotational gradient is stronger not only during the activity maxima but also during the activity minima when there are no strong magnetic fields on the solar surface. The gradient enhancement in the leptocline in quiet-Sun regions was previously noticed in the ring-diagram data^[23].

4. Variations of the Helioseismic Radius of the Sun With Respect to the Leptocline

The solar-cycle variations of the Sun's rotation rate and its gradient in the NSSL and the leptocline are accompanied by structural changes related to the dynamo-generated magnetic fields emerging on the solar surface. The subsurface magnetic field has not been measured by helioseismology, although the first attempts to detect magnetic field signatures in the acoustic travel times have been made^[29]. In general, the travel times and oscillation frequencies of acoustic waves (p-modes) depend on variations of both the magnetic field strength and temperature and their effects are not easy to separate in variations of the acoustic wave speed measured by helioseismology^{[30][31]}.

It was noticed that the frequencies of surface gravity waves (defined as f-mode of solar oscillations) predominantly depend on the gravity acceleration on the solar surface and, thus, provide a measure of the solar radius, the so-called solar helioseismic (or seismic) radius of the Sun^[17]. Comparisons of the observed f-mode frequencies with the frequencies of the standard solar model^[32] calibrated to the solar radius determined from optical observations showed a significant difference, indicating that the standard value of the solar radius must be reduced by about 300 km^{[17][33]}. This result was later confirmed by analyses of p-mode frequencies^{[34][2]}. A possible explanation is that the optical observations based on determining the position of the solar limb may be inaccurate due to the radiative transfer effects^[35] or uncertainty due to differences in the definition of the solar radius^[36].

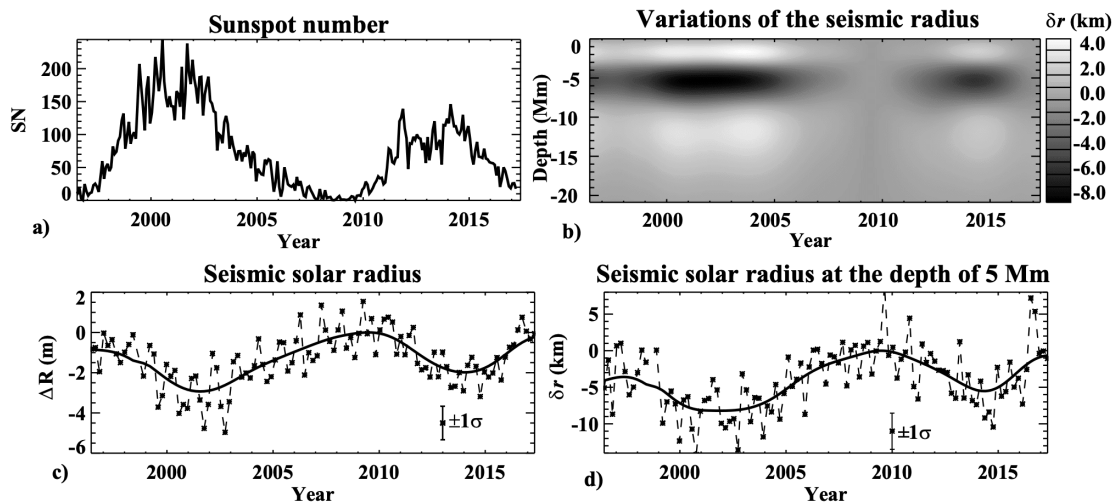


Figure 5. Variations of the seismic radius of subsurface layers during Solar Cycles 23 and 24: a) the sunspot number of these cycles; b) the time-depth diagram of subsurface displacements, δr , inferred from f-mode frequencies obtained from the SoHO and SDO data; c) the variations of the Sun's seismic radius obtained by averaging the displacements of the depth; d) the variations of the seismic radius (δr) in the leptocline, at a depth of 5 Mm. The data are adapted from Kosovichev and Rozelot^[37].

Further observations revealed variations of the seismic radius with the solar cycle, resulting in a reduction by several km with an increase in solar activity^[38]. Using nine years of data from SoHO, Lefebvre and Kosovichev^[39] established a variability of the helioseismic radius in antiphase with the solar activity, decreasing by about 2 km at the solar maximum.

By applying a helioseismic inversion technique to the observed variations of f-mode frequencies, Kosovichev and Rozelot^[37] found that the seismic radius changes are associated with variations in the subsurface stratification (Figure 5), with the strongest variations being just below the surface, around $0.995 R_{\odot}$, that is about 3.5 Mm below the surface (Fig. 5d). In addition, the radius of the deeper layers of the Sun, between 0.975 and $0.99 R_{\odot}$ changed in phase with the 11-year cycle. The variations of the displacement of the subsurface layers, δr , are illustrated in the time-depth diagram in Figure 5b. Such variations in the leptocline stratification can be caused by subsurface magnetic fields and changes in the temperature distribution.

5. Radiative Hydrodynamics Simulations of the Leptocline

Kitiashvili et al.^[12] analyzed realistic 3D radiative hydrodynamics simulations of solar subsurface dynamics in the presence of rotation in a local domain 80 Mm wide and 25 Mm deep, located at 30 degrees latitude. The simulations revealed the development of a shallow 8-Mm deep substructure of the Near-Surface Shear Layer (NSSL), characterized by strong turbulent flows and radial rotational gradient corresponding to the leptocline (Fig. 6). It is located in the hydrogen ionization zone associated with enhanced anisotropic overshooting of convective flows (revealed by enhanced fluctuations of density, ρ'_{RMS} in Fig. 6b) into a less convectively unstable layer at a depth of about 8-12 Mm between the HI/He I and He II ionization zones, as illustrated by the adiabatic exponent Γ_1 in Fig. 6a.

The overshooting is characterized by intensified turbulent mixing. The azimuthal rotational velocity sharply decreases with depth by ≈ 38 m/s in the leptocline. The gradient of rotation, $d\log \Omega / d\log r$, is about -1 in the NSSL below the leptocline and decreases to about -4 in the leptocline in agreement with observations. The simulations show a sharp increase of the gradient in a 2 Mm layer close to the surface in agreement with the helioseismic ring-diagram inferences^[3].

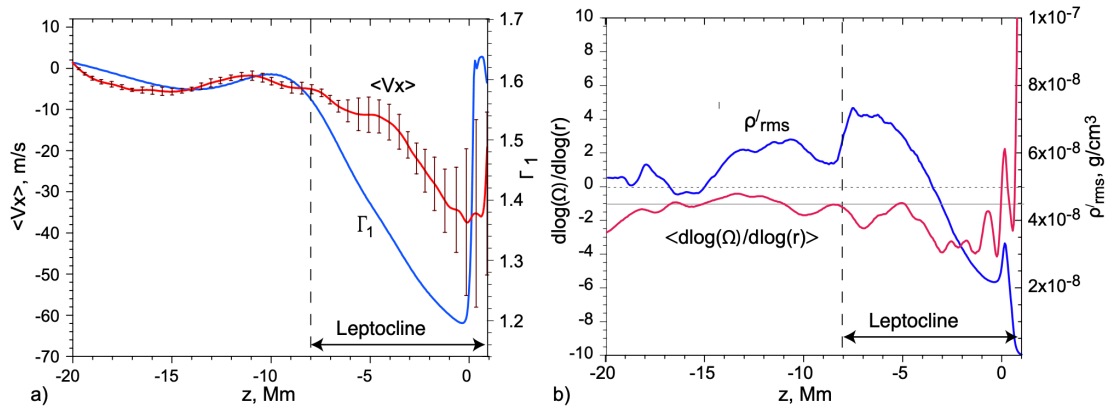


Figure 6. Mean radial profiles of a) deviations of the azimuthal flow speed from the imposed rotation rate at 30 degrees latitude (red curve) and the adiabatic index, Γ_1 (blue curve); b) the radial gradient of the rotation rate, defined as $\partial \log \Omega / \partial \log r$ (red curve), and the RMS density perturbations, ρ'_{rms} (blue curve). Radial profiles are obtained by averaging a 24-hour series of 3D simulation data horizontally over the simulation domain and in time. The vertical bars show 1σ flow velocity deviations from the mean values. The data in this figure are adapted from^[12].

6. Conclusions

In summary, the results of global and local helioseismology as well as 3D radiative hydrodynamic simulations show that the near-surface rotational shear layer (NSSL) occupying the top 15% of the solar convection zone, the depth range $\approx 30 - 35$ Mm) has a distinct substructure, the leptocline, which is about 8 Mm deep and characterized by enhanced turbulent convection and a sharp increase in the rotational shear.

The radial gradient of the solar rotation rate, $d\log \Omega / d\log r$, varies with the solar cycle. It is enhanced in regions of sunspot and active region formation. In middle and low latitudes, the gradient enhancements below the leptocline follow the magnetic butterfly diagram. However, in the leptocline, the latitudinal patterns of the enhanced gradient are more complicated, resembling the overlapping “extended” solar cycles of the torsional oscillations. Curiously, the solar-cycle variations of the radial displacement of the subsurface layers, obtained from helioseismic inversion of f-mode (surface gravity waves) frequencies, are the strongest in the middle of the leptocline, at ≈ 5 Mm. The physical mechanism of the observed solar-cycle variations may be related to the accumulation of turbulent magnetic fields in this layer and associated changes in the temperature structure.

High-resolution, realistic 3D hydrodynamic simulations reproduced the NSSL and the leptocline and showed that the rotational gradient might be stronger than found in the helioseismic inversions where the inferred rotation rate is smoothed within the averaging kernels. The simulations indicated that the origin of the leptocline is probably related to enhanced anisotropic turbulent convective downdrafts in the HI/He I ionization zone, which form an overshooting-type layer at the bottom of this zone at a depth of around 8 Mm (between the HI/He I and He II ionization zones), where turbulent mixing is intensified. It will be important to develop a synergy of helioseismic observations and numerical simulations for further understanding the complex turbulent physics of the leptocline and its role in the Sun's magnetic activity.

Acknowledgements

The work was partially supported by NASA grants: 80NSSC19K0268, 80NSSC20K1320, and 80NSSC20K0602.

References

1. [△]Howard RF. *Solar active regions as diagnostics of subsurface conditions. Annual Review of Astronomy and Astrophysics.* 1996;34:75–109. doi:10.1146/annurev.astro.34.1.75.
2. ^{a, b}Choudhuri AR, Jha BK. *The near-surface shear layer (NSLL) of the Sun: A theoretical model. Proceedings of IAUS.* 2023;365:4.
3. ^{a, b, c, d}Rabello Soares MC, Basu S, Bogart RS. *Exploring the substructure of the near-surface shear layer of the Sun. ApJ.* 2024;967(2):143.
4. [△]Kitchatinov LL. *Origin of the near-surface shear layer of solar rotation. Astron. Lett.* 2023;49:754–761. doi:10.1134/S106377372311004X.
5. ^{a, b}Vasil GM, Lecoanet D, Augustson K. (2024). "The solar dynamo begins near the surface". *Nature.* 629 (8013): 769–772. doi:10.1038/s41586-024-07315-1.
6. [△]Javaraiah J, Gokhale MK. *The Sun's rotation. New York: Nova Science; 2002.*
7. [△]Javaraiah J. *Long-term variations in the solar differential rotation. Solar Physics.* 2003;212(1):23–49.
8. [△]Tassoul JL. (2000). *Stellar rotation. Cambridge University Press, 240 p.*
9. [△]Howe R. *Solar rotation. In: Monteiro MJPF, García RA, Christensen-Dalsgaard J, McIntosh SW, editors. Dynamics of the Sun and Stars. Astrophysics and Space Science Proceedings.* 2020;57. doi:10.1007/978

10. [△]Spiegel EA, Zahn JP. (1992). "The solar tachocline". *Astronomy and Astrophysics*. 265: 106–114.
11. [△]Pipin VV, Kosovichev AG, Tomin VE. Effects of emerging bipolar magnetic regions in mean-field dynamo model of solar cycles 23 and 24. *ApJ*. 2023;949(1):7.
12. ^{a, b, c}Kitiashvili IN, Kosovichev AG, Wray AA, Sadykov VM, Guerrero G. Leptocline as a shallow substructure of near-surface shear layer in 3d radiative hydrodynamic simulations. *Monthly Notices of the Royal Astronomical Society*. 2023;518(1):504–512. doi:10.1093/mnras/stac2946.
13. [△]Godier S, Rozelot JP. A new outlook on the "differential theory" of the solar quadrupole moment and oblateness. *Sol. Phys.*. 2001;199:217. doi:10.1023/A:1010354901960.
14. [△]Scherrer PH, Bogart RS, Bush RI, et al. The solar oscillations investigation - Michelson Doppler Imager. *Solar Physics*. 1995;162(1-2):129–188. doi:10.1007/BF00733429.
15. [△]Scherrer PH, Schou J, Bush RI, et al. (2012). "Design and ground calibration of the Helio-Seismic and Magnetic Imager (HMI) instrument on the Solar Dynamics Observatory (SDO)". *Solar Physics*. 275 (1-2): 229–259. doi:10.1007/s11207-011-9842-2.
16. [△]Hill F, Stark PB, Stebbins RT, Anderson ER, Antia HM, Brown TM, Duvall TL Jr, Haber DA, Harvey JW, Hathaway DH, Howe R, Hubbard RP, Jones HP, Kennedy JR, Korzennik SG, Kosovichev AG, Leibacher JW, Libbrecht KG, Pintar JA, Rhodes EJ Jr, Schou J, Thompson MJ, Tomczyk S, Toner CG, Toussaint R, Williams WE. The solar acoustic spectrum and eigenmode parameters. *Science*. 1996;272(5266):1292–1295.
17. ^{a, b, c}Schou J, Kosovichev AG, Goode PR, Dziembowski WA. (1997). "Determination of the sun's seismic radius from the SoHO Michelson Doppler Imager". *Astrophysical Journal Letters*. 489: L197. doi:10.1086/31678.
18. [△]Larson TP, Schou J. Global-mode analysis of full-disk data from the michelson doppler imager and the helioseismic and magnetic imager. *Sol Phys*. 2018;293(2):29. doi:10.1007/s11207-017-1201-5.
19. ^{a, b, c}Schou J, Antia HM, Basu S, Bogart RS, Bush RI, Chitre SM, Christensen-Dalsgaard J, Di Mauro MP, Dziembowski WA, Eff-Darwich A, Gough DO, Haber DA, Hoeksema JT, Howe R, Korzennik SG, Kosovichev AG, Larsen RM, Pijpers FP, Scherrer PH, Sekii T, Tarbell TD, Title AM, Thompson MJ, Toomre J. (1998). "Helioseismic studies of differential rotation in the solar envelope by the solar oscillations investigation using the Michelson Doppler Imager". *ApJ*. 505 (1): 390–417.
20. [△]Thompson MJ, Toomre J, Anderson ER, Antia HM, Berthomieu G, Burtonclay D, Chitre SM, Christensen-Dalsgaard J, Corbard T, De Rosa M, Genovese CR, Gough DO, Haber DA, Harvey JW, Hill F, Howe R, Korzennik SG, Kosovichev AG, Leibacher JW, Pijpers FP, Provost J, Rhodes EJ, Schou J, Sekii T, Stark PB, Wils

- on PR. (1996). "Differential rotation and dynamics of the solar interior". *Science*. 272 (5266): 1300–1305.
21. [△]Kosovichev AG, Schou J, Scherrer PH, et al. Structure and rotation of the solar interior: Initial results from the MDI medium-l program. *Solar Physics*. 1997;170:43. doi:10.1023/A:1004949311268.
 22. [△]Gough DO, Kosovichev AG. An attempt to measure latitudinal variation of the depth of the convection zone. In: Hoeksema JT, Domingo V, Fleck B, Battrick B, editors. *Helioseismology*. 1995;376:47.
 23. ^{a, b, c}Komm R. Radial gradient of the solar rotation rate in the near-surface shear layer of the sun. *Frontiers in Astronomy and Space Sciences*. 2022;9. doi:10.3389/fspas.2022.1017414.
 24. [△]Howard R, Labonte BJ. The Sun is observed to be a torsional oscillator with a period of 11 years. *Astrophysical Journal Letters*. 1980;239:L33–L36. doi:10.1086/183286.
 25. [△]Wilson PR, Altrocki RC, Harvey KL, Martin SF, Snodgrass HB. (1988). "The extended solar activity cycle". *Nature*. 333 (6175): 748–750.
 26. [△]Kosovichev AG, Pipin VV. Dynamo wave patterns inside of the sun revealed by torsional oscillations. *ApJ*. 2019;871(2):L20.
 27. [△]Mandal K, Kosovichev AG, Pipin VV. Helioseismic properties of dynamo waves in the variation of solar differential rotation. *ApJ*. 2024;973(1):36.
 28. [△]Pipin VV, Kosovichev AG. On the origin of solar torsional oscillations and extended solar cycle. *ApJ*. 2019;887(2):215.
 29. [△]Stefan JT, Kosovichev AG. (2023). "Exploring the connection between helioseismic travel time anomalies and the emergence of large active regions during solar cycle 24". *ApJ*. 948 (1): 1.
 30. [△]Kosovichev AG, Duvall TL Jr, Scherrer PH. Time-distance inversion methods and results – (invited review). *Sol. Phys.*. 2000;192:159–176.
 31. [△]Dziembowski WA, Goode PR. Helioseismic probing of solar variability: The formalism and simple assessments. *ApJ*. 2004;600(1):464–479.
 32. [△]Christensen-Dalsgaard J, Dappen W, Ajukov SV, Anderson ER, Antia HM, Basu S, Baturin VA, Berthomieu G, Chaboyer B, Chitre SM, Cox AN, Demarque P, Donatowicz J, Dziembowski WA, Gabriel M, Gough DO, Guenther DB, Guzik JA, Harvey JW, Hill F, Houdek G, Iglesias CA, Kosovichev AG, Leibacher JW, Morel P, Proffitt CR, Provost J, Reiter J, Rhodes EJ Jr, Rogers FJ, Roxburgh IW, Thompson MJ, Ulrich RK. The current state of solar modeling. *Science*. 1996;272(5266):1286–1292.
 33. [△]Antia HM. Estimate of solar radius from f-mode frequencies. *Astronomy and Astrophysics*. 1998;330:336–340. doi:10.48550/arXiv.astro-ph/9707226.

34. [△]Kholikov S, Hill F. *Sol. Phys.*. 2008;251(1-2):157–161. doi:10.1007/s11207-008-9205-9.
35. [△]Haberreiter M, Schmutz W, Kosovichev AG. Solving the discrepancy between the seismic and photospheric solar radius. *ApJ*. 2008;675(1):L53.
36. [△]Rozelot JP, Kosovichev A, Kilcik A. Solar radius variations: new look on the wavelength dependence. In: Kosovichev AG, Hawley SL, Heinzel P, editors. *Solar and Stellar Flares and their Effects on Planets*. 2016; 320:342–350.
37. [△][△]Kosovichev AG, Rozelot JP. Cyclic changes of the Sun's seismic radius. *The Astrophysical Journal*. 2018;861(2):id. 90. doi:10.3847/1538-4357/aac81d.
38. [△]Dziembowski WA, Goode PR, di Mauro MP, Kosovichev AG, Schou J. Solar cycle onset seen in Soho Michelson Doppler Imager seismic data. *ApJ*. 1998;509(1):456–460.
39. [△]Lefebvre S, Kosovichev AG. Changes in the subsurface stratification of the sun with the 11-year activity cycle. *The Astrophysical Journal*. 2005;633(2):L149–L152. doi:10.1086/498305.

Declarations

Funding: The work was partially supported by NASA grants: 80NSSC19K0268, 80NSSC20K1320, and 80NSSC20K0602.

Potential competing interests: No potential competing interests to declare.